

Regulation of Myosin V Processivity by Calcium at the Single Molecule Level^{*S}

Received for publication, May 30, 2006, and in revised form, August 11, 2006 Published, JBC Papers in Press, August 18, 2006, DOI 10.1074/jbc.M605181200

Hailong Lu, Elena B. Kremtsova, and Kathleen M. Trybus¹

From the Department of Molecular Physiology and Biophysics, University of Vermont, Burlington, Vermont 05405

Calcium can affect myosin V (myoV) function in at least two ways. The full-length molecule, which adopts a folded inhibited conformation in EGTA, becomes extended and active in the presence of calcium. Calcium also dissociates one or more calmodulin molecules from the extended neck. Here we investigated at the single molecule level how calcium regulates the processive run length of full-length myosin V (dFull) and a truncated dimeric construct (dHMM), which cannot adopt the folded conformation. The processivity of dFull and dHMM is tightly controlled by the calcium and calmodulin concentration, with shorter runs occurring at higher calcium concentration. The data indicate that a calcium-dependent dissociation of calmodulin from the neck region of myoV terminates its processive run. dFull showed unexpected processive movement in EGTA, suggesting that a small population of extended, active molecules are in equilibrium with the inhibited, folded form. Single turnover assays showed that the ATPase activity of the folded full-length molecule is inhibited by more than 50-fold compared with the extended molecule. The results imply that activation and termination of the processive runs of myoV can be accomplished by multiple mechanisms.

Myosin V (myoV)² is a processive motor capable of taking multiple steps on actin filaments before dissociation (1). A striking feature of the molecule is its extended neck region which binds 6 calmodulins (CaM) and acts as a lever arm. This long neck region enables myoV to take 36-nm steps along the actin filament through a hand-over-hand mechanism (2), mediated by strain between the two heads (reviewed in Ref. 3). In addition to the widely accepted mechanical role of the lever arm, it is likely that the neck may also be involved in the regulation of myoV activity, given that CaM is a universal calcium sensor. Each CaM binds to an "IQ motif," with a consensus sequence of IQXXRGXXXR, where *X* denotes any amino acid.

In the absence of calcium, the IQ motifs are fully occupied by CaM. In the presence of calcium, one or more CaM molecules dissociate from the neck (4–6). Based on data obtained with truncated neck constructs, it is likely that calcium-CaM can dissociate from the second IQ motif relative to the motor domain (5, 7).

The actin-activated ATPase activity of full-length myoV, but not of shorter dimeric constructs, is inhibited in the absence of calcium and activated in its presence. Accompanying the activity change is a conformational change from a folded (inhibited) to an extended (active) conformation, which is seen only with the full-length molecule (5, 8, 9). Recent three-dimensional reconstructions of crystalline arrays of the folded form of myoV revealed structural details of the inhibited state (10). In this model, the molecule bends at the junction of the sixth IQ motif and the α -helical coiled-coil, so that the cargo-binding globular tail docks onto the two motor domains. The site of interaction is near loop 1 at the entrance to the nucleotide binding pocket, thus providing a possible structural mechanism for the reduced ATPase activity in the inhibited state.

Actin-activated ATPase activity is in accord with this calcium-dependent transition from an inhibited to an active state, but it is puzzling that full-length myoV shows such good *in vitro* ensemble motility in EGTA (5, 11). This observation might be reconciled by unfolding and activation of the molecule upon binding to the nitrocellulose-coated surface of the flow cell. In single molecule processivity assays, however, the actin filament is immobilized on the surface, and myoV is free in solution. In this case, processive runs of full-length myoV in EGTA cannot be explained by "cargo" activation (2, 12). Provided that the fluorescently labeled CaM used to visualize the myoV does not preclude formation of the inhibited state, there is no convincing explanation for processive runs of the full-length molecule in EGTA.

In addition to calcium regulation of the conformational state of full-length myoV, calcium also dissociates CaM from one or more of the IQ motifs. Ensemble motility assays showed reduced or no motility in the presence of calcium (5, 11), which could be rescued by the addition of extra CaM. This implies that CaM dissociation inhibits motility. The two effects of calcium on myoV function, one activating (ATPase activity) and one inhibitory (motility), appear in contradiction to each other. Moreover, because myoV is thought to transport cargo processively as a single molecule, ensemble motility experiments are only a first step toward understanding the *in vivo* regulation of myoV by calcium.

Here we used a single molecule total internal reflection fluorescence (TIRF) microscopy assay to assess the processivity of

* This work was supported by National Institutes of Health Grant HL38113 (to K. M. T.). The costs of publication of this article were defrayed in part by the payment of page charges. This article must therefore be hereby marked "advertisement" in accordance with 18 U.S.C. Section 1734 solely to indicate this fact.

^S The on-line version of this article (available at <http://www.jbc.org>) contains supplemental material including Table 1s and Fig. 1s.

¹ To whom correspondence should be addressed: Dept. of Molecular Physiology and Biophysics, University of Vermont, 149 Beaumont Ave., Burlington, VT 05405. Tel.: 802-656-8750; Fax: 802-656-0747; E-mail: kathleen.trybus@uvm.edu.

² The abbreviations used are: myoV, myosin V; CaM, calmodulin; HMM, heavy meromyosin; dHMM, dilute HMM (a truncated double-headed myoV construct); dFull, dilute full-length myoV; TIRF, total internal reflection fluorescence; YFP, yellow fluorescent protein.

full-length myoV and a truncated double-headed molecule as a function of calcium concentration. These two constructs allowed us to distinguish the effect of calcium on CaM dissociation, which is common to both constructs, *versus* calcium unfolding of the inhibited form, which is unique to the full-length construct. Both HMM and full-length myoV show shorter processive run lengths in calcium despite the presence of exogenous CaM, suggesting that transient dissociation of CaM ends the processive run of a single motor. The majority of full-length myoV in EGTA is folded, not processive, and has an ATPase activity that is inhibited at least 50-fold compared with the active state. A small fraction of extended full-length molecules in EGTA showed processivity at normal speeds. The picture that emerged is that both activation and termination of a processive run can occur by multiple mechanisms, which will depend on the interplay among calcium, CaM, and cargo concentration.

MATERIALS AND METHODS

Proteins—Full-length myoV (dFull, 1877 amino acids, with exons A, C, D, E, and F in the tail) and a truncated dimer (dHMM, 1098 amino acids) were expressed with or without yellow fluorescent protein (YFP) at the C terminus. All constructs contained a FLAG epitope (DYKDDDDK) at the C terminus to facilitate purification by affinity chromatography. Expression in the Sf9 insect cell/baculovirus system and protein purification is essentially as described before (5). Full-length myoV was further purified by ion-exchange fast performance liquid chromatography on a 1-ml MonoQ 5/50 GL column on the AktaFPLC (GE Healthcare). The protein was applied in 10 mM Hepes, pH 7.4, 1 mM EGTA, 200 mM NaCl and eluted with 20 column volumes of a salt gradient from 200 to 600 mM NaCl at 0.5 ml/min. Minor proteolytic products eluted at a lower salt concentration than the intact heavy chain, which eluted near the end of the gradient. Calmodulin was expressed and purified as described previously (5). Chicken skeletal actin was prepared from acetone powder (13) and labeled with phalloidin-Alexa 660 (Invitrogen).

Processivity Assay by Single Molecule TIRF Microscopy—Single molecule motility assays were performed at room temperature ($25 \pm 1^\circ\text{C}$) on a Nikon TE2000-U microscope equipped with a PlanApo objective lens ($\times 100$; numerical aperture, 1.45) for through-the-objective TIRF microscopy as described previously (14). For TIRF assays, flow cells were first incubated with 0.1 mg/ml *N*-ethylmaleimide-modified myosin for 2 min, rinsed with buffer A (25 mM imidazole, pH 7.4, 4 mM MgCl_2 , 1 mM EGTA, 25 mM KCl, 10 mM dithiothreitol), incubated with 0.5 μM Alexa 660-phalloidin-labeled actin filaments for 2 min, and then rinsed with buffer B which contained buffer A plus 12 μM CaM, 1 mM ATP, an oxygen scavenger system (3 mg/ml glucose, 0.1 mg/ml glucose oxidase, 0.18 mg/ml catalase), an ATP regenerating system (0.5 mM phosphoenolpyruvate and 100 units/ml pyruvate kinase), and various amounts of Ca^{2+} to achieve the desired free Ca^{2+} . The ratio of EGTA: Ca^{2+} needed to obtain a specific free Ca^{2+} concentration was calculated with Webmaxclite V1.15. The free calcium concentrations of the buffers were verified independently with two fluorescent calcium indicators (calcium green-2 and calcium green-5N) from

Molecular Probes following the manufacturer's protocols. The myoV was diluted to final concentration of 0.3–1.0 nM in buffer B and added to the flow cell. Experiments measuring dHMM processivity in 1 μM Ca^{2+} without extra CaM were carried out as described above except that there was no CaM in buffer B.

Data acquisition and processing were essentially the same as described previously (14). Here we required that each trajectory be longer than 0.5 μm to be considered a valid processive run. This was based on our criteria that a molecule moves continuously for at least four frames, which enabled us to distinguish directed movement from Brownian motion, as discussed in detail by Kremenitsova *et al.* (14). The results were a file containing the run length and speed for all the individual myoV processive runs. The run lengths were then combined into a histogram with a bin size of 0.2 μm . The run length distribution histogram was fit with

$$p(x) = Ae^{(-x/\lambda)} \quad (\text{Eq. 1})$$

to determine the characteristic run length λ , where $p(x)$ is the probability of the myosin traveling a distance x along an actin filament and A is a constant.

Our characteristic run lengths for dHMM and dFull are shorter than those reported by others under similar conditions ($\approx 1\text{--}2 \mu\text{m}$) (15, 16). A major difference is that the earlier data were analyzed by hand, whereas we used an automated tracking program. The automated program tends to result in shorter run lengths because it is better than humans at detecting short runs and also because the YFP fluorescence emission occasionally flickers. If the fluorescence intensity flickers in the middle of a run, the tracking program will occasionally count this as two short runs, whereas a human analyzing the data will count this as one long run. The photobleaching rate of YFP, which was determined to be $\approx 0.1 \text{ s}^{-1}$, did not significantly affect our observations.

Kinetic Assays—The stop-flow experiments were carried out on a Kintek SF-2002 stop-flow apparatus (Kintek, Austin, TX). All kinetic measurements were carried out in a buffer containing 10 mM Hepes, pH 7.4, 4 mM MgCl_2 , and 50 mM KCl at 20°C . 2',3'-mantATP and 2',3'-mantADP were purchased from Invitrogen. 3'-*O*-(*N*-Methylanthraniloyl)-2'-deoxyadenosine 5'-triphosphate (mant-dATP) was purchased from Jena Biosciences. The mant fluorophore was excited at 360 nm (10-nm bandwidth), and emission monitored with a 400-nm cutoff filter. Single ATP turnover experiments were carried out with a double mixing protocol. Briefly, 0.2 mg/ml myoV (dFull or dHMM) in 3 mM EGTA or 300 μM Ca^{2+} was first mixed with a 2.2 molar ratio of mantATP and then allowed to age for 5–15 s to form the ADP· P_i complex. The myosin·ADP· P_i was then mixed with a solution containing various concentrations of actin and 3 mM MgATP.

The rate of ADP release was measured by mixing a solution containing 0.2 mg/ml myosin, a 2.2 molar excess of 2',3'-mantADP, and a 1.5-fold molar excess of actin with a solution containing 4 mM MgADP. MantATP binding to myoV was done with a single mixing protocol. Briefly, 0.2 mg/ml myoV (dFull or dHMM) in 2 mM EGTA or 200 μM Ca^{2+} was mixed with various concentrations of mantATP. The fluorescence

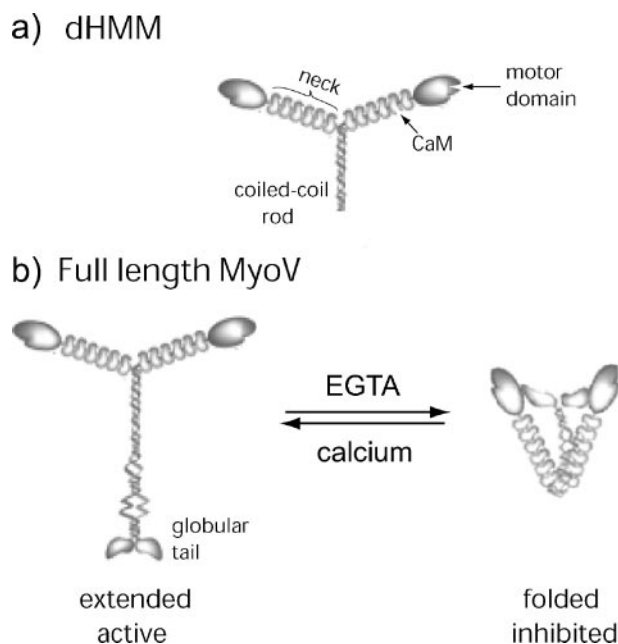


FIGURE 1. **Schematic diagram of the two constructs used in this study.** *a*, truncated dHMM. *b*, full-length myoV in its active, extended conformation (*left*) or its folded, inhibited conformation (*right*).

traces were fit to 1, 2, or 3 exponentials using software provided by Kintek.

Steady-state actin-activated ATPase assays were performed at 20 °C in 10 mM imidazole, pH 7.0, 50 mM KCl, 1 mM MgCl₂, 1 mM EGTA (or 100 μM Ca²⁺), 1 mM dithiothreitol, 1 mM MgATP, and 12 μM exogenous CaM. The buffers also contained an ATP regenerating system (0.5 mM phosphoenolpyruvate, 100 units/ml pyruvate kinase), 0.2 mM NADH, and 20 units/ml lactate dehydrogenase. The rate of the reaction was measured from the decrease in absorbance at 340 nm. Data were fit to the Michaelis-Menten equation to obtain V_{\max} and K_m . ATPase rates (s⁻¹) correspond to turnover rate/head.

RESULTS

Expressed Constructs—A murine full-length myoV (dFull) and a truncated dimeric construct (dHMM), with or without YFP at the C terminus of the heavy chain, were expressed using the baculovirus/insect cell system. Fig. 1 shows a schematic of the two constructs. YFP served as the fluorophore for single molecule studies. Constructs without YFP were used for transient kinetic studies so that YFP did not interfere with the fluorescent mantATP signal. Typical yields were ≈ 1–3 mg of protein/billion cells.

Effect of Calcium on dHMM Processivity—Experiments were first performed with dHMM, which does not form a folded, inhibited conformation. The processivity of dHMM-YFP was determined using a TIRF microscopy assay in which YFP-labeled myoV constructs were visualized moving on immobilized fluorescently labeled actin filaments. At 1 nM dHMM in the presence of EGTA, numerous processive runs were observed over several minutes. At the same concentration of dHMM in the presence of 1 μM Ca²⁺, no processive movement was observed. We required that each trajectory be longer than 0.5 μm to be considered a valid processive run (see “Materials and

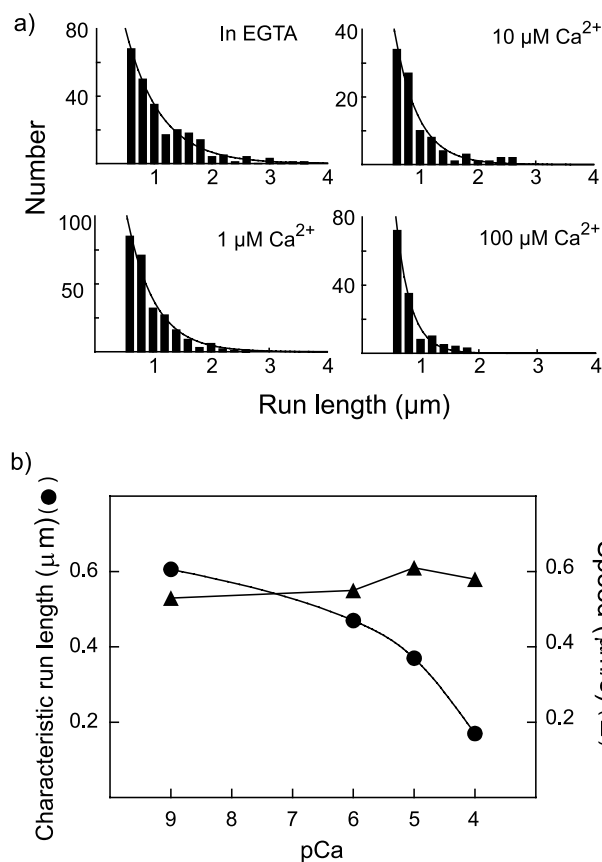


FIGURE 2. **Characteristic run length of dHMM at different calcium concentrations.** *a*, histograms of dHMM run length at the indicated calcium concentrations in the presence of 12 μM CaM. The solid curves are fitted to Equation 1, $p(x) = Ae^{(-x/\lambda)}$, where λ is the characteristic run length (see “Materials and Methods”). Data from two protein preparations were pooled to generate each histogram. *b*, the calcium dependence of speed and characteristic run length of dHMM. Velocity values from two preparations were averaged.

Methods”). Repetition of the experiment at higher dHMM concentrations still showed no processive runs. Extra CaM was not included in these assays.

The processivity of dHMM-YFP was then investigated in the presence of 12 μM CaM as a function of calcium concentration (0, 1, 10 and 100 μM Ca²⁺). Processive runs were observed at all calcium concentrations tested (Fig. 2*a*). The run length data were analyzed as described under “Materials and Methods.” The velocity and characteristic run lengths for dHMM at each calcium concentration are shown in Fig. 2*b*. The velocities are ≈ 0.55 μm/s for all calcium concentrations tested, similar to the value reported previously (14). In contrast, the characteristic run length decreased with increasing calcium concentration. At 100 μM calcium, the characteristic run length was only ≈ 0.17 μm, despite the presence of exogenous CaM. The reduced run length was not due to a decreased ATPase activity, because the speed was constant.

Longer processive runs could be restored by calcium removal. Run lengths were first measured in 100 μM calcium with extra CaM, conditions under which dHMM showed short processive runs. Enough 100 mM EGTA was then added into the flow cell to chelate all of the calcium, and the characteristic run length was remeasured. Run lengths were restored to a level

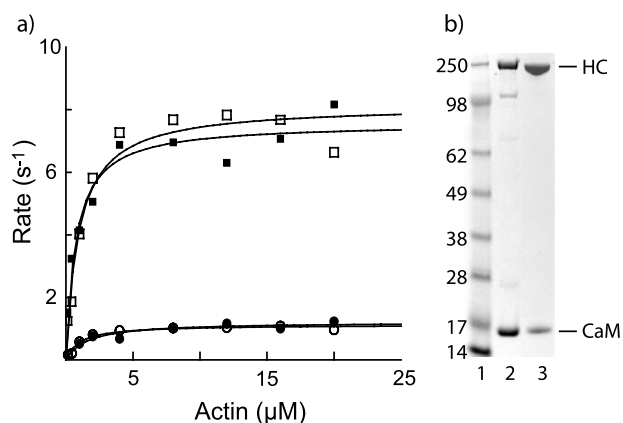


FIGURE 3. *a*, actin-activated ATPase activity of the full-length construct with (open symbols) or without (filled symbols) YFP at the C terminus. Values obtained in EGTA are shown by circles, and values obtained in 100 μM Ca^{2+} are shown by squares. V_{max} and K_m values are as follows: dFull in calcium ($7.57 \pm 0.34 \text{ s}^{-1}$ and $0.73 \pm 0.16 \mu\text{M}$); dFull-YFP in calcium ($8.15 \pm 0.37 \text{ s}^{-1}$ and $0.95 \pm 0.21 \mu\text{M}$); dFull in EGTA ($1.22 \pm 0.09 \text{ s}^{-1}$ and $1.57 \pm 0.55 \mu\text{M}$); dFull-YFP in EGTA ($1.13 \pm 0.04 \text{ s}^{-1}$ and $1.01 \pm 0.17 \mu\text{M}$). ATPase rates (s^{-1}) correspond to turnover rate/head. Results from two independent preparations were similar; one preparation is shown here. *b*, 4–12% SDS-gradient gel with molecular mass standards (lane 1) and the expressed purified full-length myoV construct before (lane 2) and after (lane 3) ion exchange chromatography. Note that extra CaM was added to myoV prior to chromatography (lane 2) to ensure full occupancy of the IQ motifs. Numbers to the left of the standards show molecular mass in kDa. HC, heavy chain.

similar to that observed in a sample that had not been exposed to calcium ($\approx 0.5 \mu\text{M}$).

Effect of Calcium on the Processivity of Full-length myoV—The calcium dependence of processivity of the full-length construct was determined under the same conditions used for dHMM. We first established that the YFP tag did not interfere with the ability of the full-length construct to form the inhibited, folded conformation. The steady-state actin-activated ATPase activity of dFull and dFull-YFP was determined in the presence or absence of calcium with 12 μM exogenous CaM. In the presence of calcium, both dFull and dFull-YFP had V_{max} values of $\approx 8 \text{ s}^{-1}$ (Fig. 3*a*). In EGTA, both dFull and dFull-YFP had rates that were $\approx 1 \text{ s}^{-1}$, considerably lower than the value obtained in calcium (Fig. 3*a*). These activity measurements imply that dFull-YFP can form the inhibited conformation in EGTA to the same extent as dFull. A gel of the fast performance liquid chromatography-purified full-length myoV shows the quality of the preparation (Fig. 3*b*, lane 3).

The velocity and characteristic run length for dFull as a function of calcium concentration in the presence of excess CaM were determined (Fig. 4). The velocities are $\approx 0.41 \mu\text{m/s}$, independent of calcium concentration. In EGTA, the characteristic run length ($\approx 0.33 \mu\text{m}$) is about half that observed with dHMM. At 1 and 10 μM calcium, dFull shows processivity comparable with dHMM ($\approx 0.3 \mu\text{m}$). At 100 μM calcium, the characteristic run length is very short ($\approx 0.07 \mu\text{m}$), which is the distance traversed when myoV takes two steps. Thus, both dFull and dHMM showed reduced processivity in calcium despite the presence of excess CaM.

Full-length myoV Shows Many Fewer Runs in EGTA Compared with dHMM—The processive runs of dFull in EGTA, despite being somewhat shorter than dHMM, were unexpected because the molecule should be in the inhibited conformation

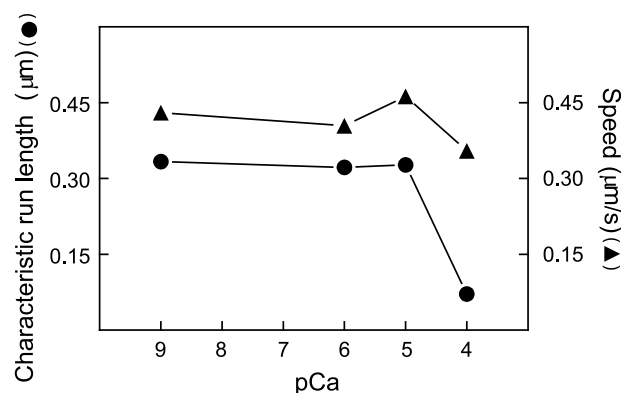


FIGURE 4. The calcium dependence of speed and characteristic run length for full-length myoV. Excess CaM (12 μM) is present in all the samples. Values from two independent preparations were averaged.

TABLE 1
Comparison of dHMM and dFull in EGTA

The concentration of dHMM and dFull was 0.35 nM.

	dHMM	dFull
Velocity ($\mu\text{m/s}$)	0.47 ± 0.10	0.48 ± 0.16
Run length (μm)	0.60	0.33
No. of runs observed/5 min	246	32

based on actin-activated ATPase measurements. The concentration of dFull and dHMM was varied in the experiments described above to get the maximum number of processive runs for analysis. Here, we matched the concentration of dHMM and dFull at 0.35 nM under identical buffer conditions. In the same period of recording (5 min) for each species, we observed 246 processive runs for dHMM but only 32 runs for dFull (Table 1). Only a small fraction of the full-length molecules ($\approx 13\%$) could sustain processive runs, consistent with the majority of the population being in a folded conformation that is not capable of processive motion. This experiment involved several assumptions because we were comparing a truncated and a full-length construct. Nonetheless, the fraction of extended full-length molecules deduced from the single molecule experiment agreed well with the actin-activated ATPase results, which imply that $\approx 12\%$ of the full-length molecules are active (see above and the supplemental material).

Single Turnover Rates Show a High Degree of Regulation for dFull—Single turnover experiments were performed in EGTA or 100 μM calcium as a function of actin concentration. MyoV was mixed with mantATP, aged to form the ADP \cdot P $_i$ complex, and then mixed with varying concentrations of actin and excess unlabeled ATP (Fig. 5*a*). Single turnovers ensure that the contribution of each myosin head to the total signal is equal, regardless of its rate constant. In contrast, rapidly cycling species can dominate steady-state assays by hydrolyzing multiple ATP molecules. The single isomer of mantATP (3'-mantATP) was used in some experiments, but the data were indistinguishable from those obtained using the 2',3'-mantATP mixture.

The data for dFull in EGTA were best fit to a double exponential equation. The signal with the larger amplitude ($\approx 70\text{--}80\%$ of the total) had a rate of $\approx 0.2 \text{ s}^{-1}$ and showed no actin dependence (Fig. 5*b*). This signal measures the rate of ADP release from the inhibited conformation. The data for dFull in 100 μM calcium were also best fit to a double exponential equation.

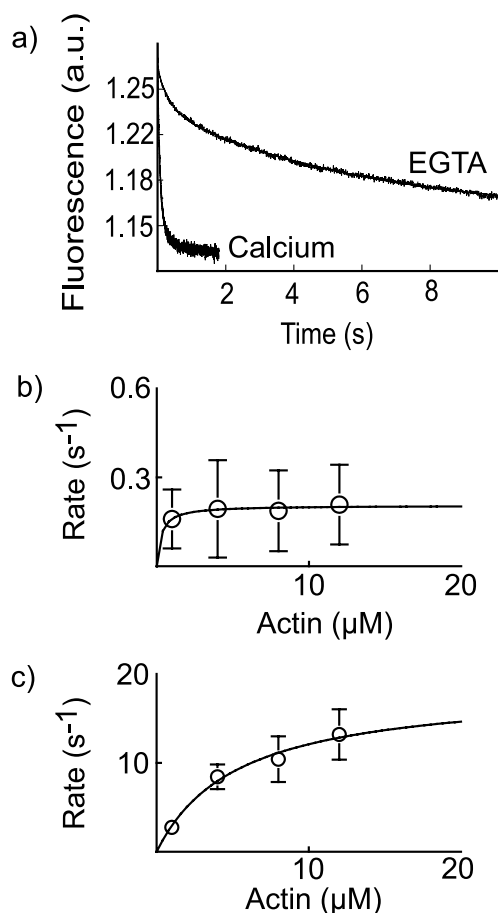


FIGURE 5. Single turnovers of ATP by dFull as a function of actin concentration. *a*, representative fluorescence decay traces, with or without calcium, at 12 μM actin. Data obtained in EGTA or calcium are plotted as a function of actin concentration in *b* and *c*, respectively. The maximum rate is $\approx 0.2 \text{ s}^{-1}$ in EGTA, and $\approx 15 \text{ s}^{-1}$ in calcium. Data were obtained from at least three experiments using two different preparations of dFull.

tion. The signal with the larger amplitude ($\approx 80\%$ of the total) was dependent on actin concentration and had a maximal rate of $\approx 15 \text{ s}^{-1}$ (Fig. 5c), which is similar to the rate reported for ADP release from an unstrained myoV head. The origin of the minor amplitude signals in EGTA and calcium is discussed in the supplemental material.

Controls performed with dHMM showed two rates that were the same in both EGTA and 100 μM calcium. At 12 μM actin, the data traces were best fit to a double exponential equation with two rates (10 and 1.5 s^{-1}) of similar amplitude. This result was expected because dHMM cannot adopt the inhibited conformation, and thus its actin-activated ATPase activity is not regulated by calcium.

Calcium Dependence of ADP Release and ATP Binding—An actin-dFull-mantADP complex was mixed with ADP to determine the rate of ADP release. In EGTA, the data were best fit to a double exponential equation with a slow rate of $\approx 0.5 \text{ s}^{-1}$ (60% amplitude) and a fast rate of $\approx 4 \text{ s}^{-1}$. In calcium, the traces were best fit to a double exponential equation with a fast rate of $\approx 12 \text{ s}^{-1}$ (75% amplitude) and a slower rate of $\approx 1.1 \text{ s}^{-1}$.

The binding of mantATP to dFull was measured. The data were best fitted to a single exponential. The rate increased almost linearly with the mantATP concentration over the range

TABLE 2
Summary of rate constants for dFull

	EGTA	Calcium
Maximal single turnover rates	$\approx 0.2 \text{ s}^{-1}$	$\approx 15 \text{ s}^{-1}$
MantADP release from myoV bound to actin	$\approx 0.5 \text{ s}^{-1}$	$\approx 12 \text{ s}^{-1}$
ATP binding	$1.4 \mu\text{M}^{-1} \text{ s}^{-1}$	$1.2 \mu\text{M}^{-1} \text{ s}^{-1}$

of 1–20 μM , defining a second order rate constant of $1.4 \mu\text{M}^{-1} \text{ s}^{-1}$ in EGTA and $1.2 \mu\text{M}^{-1} \text{ s}^{-1}$ in 100 μM calcium. A similar experiment with dHMM in EGTA gave a value of $1.4 \mu\text{M}^{-1} \text{ s}^{-1}$. Thus calcium does not regulate the rate of ATP binding. Measured rate constants are summarized in Table 2.

DISCUSSION

Full-length myoV adopts a folded, inhibited monomeric conformation in the absence of calcium, which showed no processive movement. The folded form has an actin-activated ATPase activity that is at least 50-fold lower than the extended form. The fast processive runs observed with the full-length molecule in EGTA were attributed to a small fraction of extended molecules that were in equilibrium with the folded form. The truncated dHMM molecule cannot form the folded inhibited state and is fully active even in EGTA. Low calcium concentrations unfold and activate full-length myoV, but higher calcium concentrations act as a “brake” on both dHMM and dFull processivity. We used a single molecule assay to infer that calcium-induced dissociation of CaM from either HMM or full-length myoV stops a processive run. Dissociation occurs even when excess CaM is present. Gaïting between the lead and trailing heads, mediated by strain in the CaM-containing neck, is a key feature that enables the processive movement of myoV (reviewed in Ref. 3). It is therefore not surprising that dissociation of CaM by calcium resulted in a compliant neck, causing a loss of strain-dependent communication between the two heads of myoV and a loss of the ability of myoV to continue stepping along an actin filament.

Without exogenous CaM, 1 μM calcium was sufficient to stop processive movement because CaM dissociated but did not rebind under our assay conditions. This observation argues against a model in which CaM dissociation reduces but does not eliminate processivity. Thus, when both calcium and exogenous CaM were present, short processive runs were observed because molecules that had lost CaM could also rebind it and start a processive run. A molecule that is running processively, however, is not immune to calcium binding to its bound CaM. When this happens, the Ca^{2+} -CaM binds less tightly to at least one IQ motif and dissociates, resulting in no further coordinated stepping. This molecule will finish its ATPase cycle and dissociate from actin, thus terminating its processive run. The shortened processive runs of dHMM in calcium not only showed that CaM dissociation stops processive movement but also indicated that CaM can rebind to an empty IQ motif in the myoV neck. Dissociation and rebinding is therefore reversible, as further shown by the restoration of long run lengths by calcium chelation in the presence of extra CaM. In contrast to the single molecule results obtained here, when actin movement is powered by more than one myoV molecule (*i.e.* in ensemble measurements), another motor that has retained its full com-

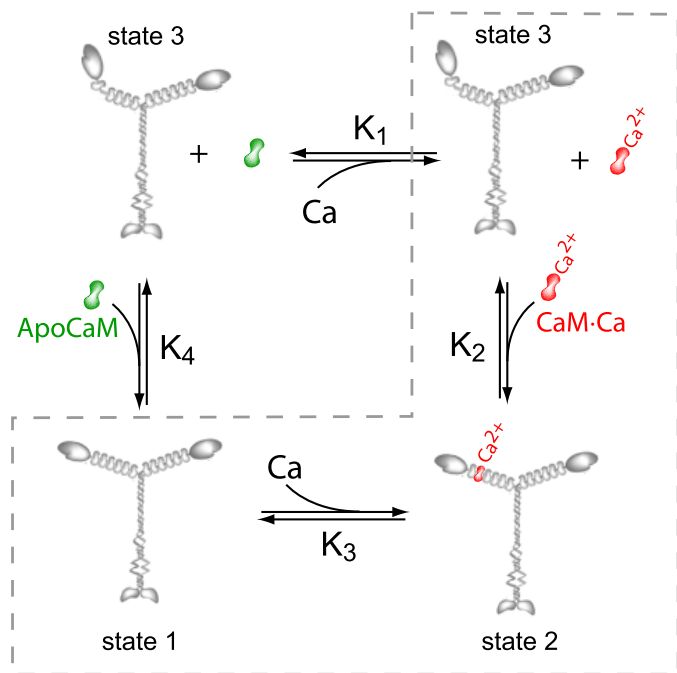


FIGURE 6. **Equilibrium between myosin, calcium, and CaM.** State 1 is extended, full-length myoV capable of processive movement along actin. State 2 is myoV with calcium-CaM bound to its neck, which is capable of processive movement. State 3 is myoV that has lost one or more CaM from its neck and is incapable of processive movement. The scheme delineated by the dashed-line box explains the calcium-dependent rate of termination of a processive run. It differs from the linked equilibria, however, in that the conversion from state 2 to state 3 is considered irreversible.

plement of CaM can sustain movement (5). If multiple motors are present on certain organelles *in vivo*, cargo delivery over long distances would be safeguarded even in the presence of calcium.

The complex relationship between calcium, CaM, and full-length myoV can be described by four equilibria (Fig. 6), which is an oversimplification because each CaM can bind a maximum of four calcium ions. These four equilibria are linked through the dissociation constants $K_1 * K_2 = K_3 * K_4$. Because at least one CaM in the myoV neck has a lower affinity for its IQ motif in the presence of calcium, $K_2 > K_4$. Therefore, $K_3 > K_1$, which implies that calcium binds more weakly to CaM bound to the myoV neck than to a free CaM. In the presence of calcium but the absence of exogenous CaM, most myoV will be in state 3, which is not processive. The myoV concentration in the TIRF assay is in the subnanomolar range, and thus the dissociated CaM concentration is negligible. With both calcium and added CaM present, the myoV will be partitioned among the three states, with the relative amount in each state depending on the four equilibrium constants.

Processivity of Full-length myoV in EGTA—Full-length myoV showed unexpected processivity in EGTA, conditions under which it adopts the inhibited, folded conformation. The fast velocity of the full-length molecule during its processive run is evidence that ATP is being hydrolyzed at the rate of an active, extended molecule, and thus we conclude that we are observing the processive movement of some unfolded full-length myoV molecules. The extended and folded conformations are therefore in equilibrium in EGTA, with the equilibrium favoring the

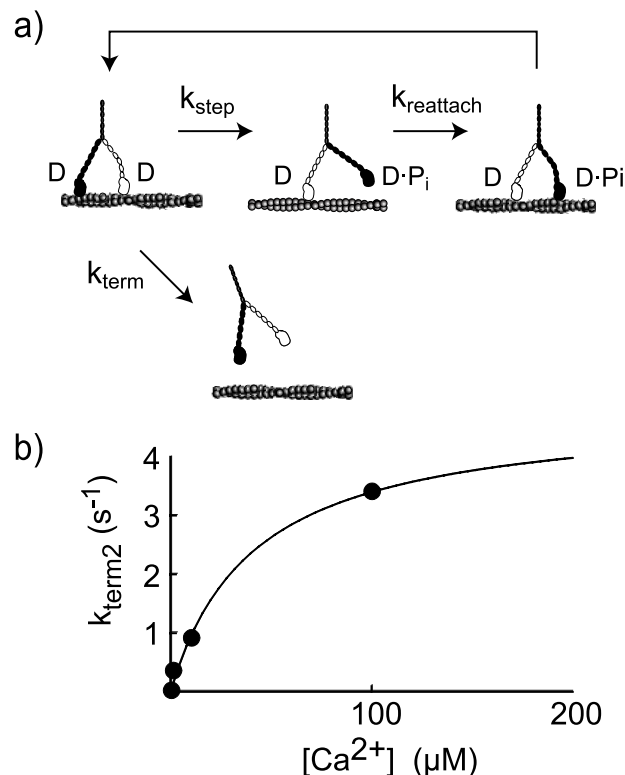


FIGURE 7. **Rates of CaM dissociation from the myoV neck by calcium.** *a*, scheme showing the processivity of myoV. The data in *b* are fitted to Equation 2.

folded conformation. The ratio of the number of runs observed from the active *versus* inhibited forms (Table 1) can then be viewed as an approximate equilibrium constant for the folded to unfolded conversion ($K \approx 8$). From this we estimate the free energy needed for this conversion as $k_B T \ln(K) \approx 2.1 k_B T$. This value is comparable with the thermal energy available to the molecule ($\approx k_B T$), and thus the estimate of 8 for the ratio of folded:unfolded molecules is likely to be an underestimation.

These processive runs cannot be due to an unregulated HMM-like cleavage product, because C-terminal cleavage will result in a loss of YFP, which will render the molecule “invisible” by TIRF microscopy. Conversely, a cleavage product that retains YFP would lack an intact motor domain. One could argue that the YFP molecule at the C terminus of the tail acts as a cargo that interferes with the tail-motor domain interaction necessary to stabilize the folded conformation. We showed, however, that the steady-state actin-activated ATPase activity of the full-length myoV-YFP construct is calcium-regulated to the same extent as the construct without YFP (Fig. 3*a*). Tissue-purified full-length myoV containing exchanged fluorescently labeled CaM also shows processive movement in EGTA (2, 12), but the possibility of an HMM-like cleavage product in these preparations cannot be ruled out. It is possible but unlikely that the fraction of full-length molecules that is extended has been modified in a way that would not be observed on a gel, such as a post-translational modification. The fairly constant ratio of activity seen in calcium *versus* EGTA argues against this possibility.

Rate of CaM Dissociation by Calcium—The processive run length of myoV decreased with increasing calcium concentra-

TABLE 3

Calculated termination rates for the model described in the text

Data from Fig. 2 obtained with dHMM were used for these calculations.

pCa	Run length (λ)	Steps (n)	Velocity (v)	k_{step}	k_{term}	k_{term1}	k_{term2}
	μm		$\mu\text{m/s}$	s^{-1}	s^{-1}	s^{-1}	s^{-1}
9	0.61	16.8	0.53	14.7	0.93	0.93	0
6	0.47	13.1	0.55	15.3	1.27	0.93	0.34
5	0.37	10.3	0.61	16.9	1.83	0.93	0.90
4	0.17	4.7	0.58	16.1	4.33	0.93	3.4

tion, and thus CaM dissociation by calcium is a second order reaction in which the rate depends on the calcium and bound CaM concentration. To extract quantitative information from these data, we used a simple scheme describing the processivity of myoV (14) (Fig. 7a). An alternative scheme, which was also described by Kremntsova *et al.* (14), yielded similar conclusions and is presented in the supplemental material.

We assume that myoV processivity has an intrinsic rate of termination (k_{term}), with $k_{\text{term}} = k_{\text{step}}/(n - 1)$. The measured parameters are velocity (v) and characteristic run length (λ). From the velocity one calculates k_{step} ($k_{\text{step}} = v/36 \text{ nm}$). From the run length one calculates n , the number of processive steps taken by myoV ($n = \lambda/36 \text{ nm}$). The parameter k_{term} can then be calculated (Table 3). We propose that k_{term} consists of two component rates, a calcium-independent intrinsic rate of dissociation of myoV (k_{term1}) and a calcium-dependent rate of CaM dissociation by calcium (k_{term2}). Because these two processes are independent of each other, $k_{\text{term}} = k_{\text{term1}} + k_{\text{term2}}$. In EGTA, $k_{\text{term2}} = 0$, so $k_{\text{term}} = k_{\text{term1}}$. The calculated rates show that k_{term2} increases with calcium concentration (Table 3). The rate of CaM dissociation at pCa 5.2 was measured at $\approx 0.4 \text{ s}^{-1}$ in a recent study (6), which is quite similar to our results.

A plot of k_{term2} as a function of calcium concentration (Fig. 7b) shows that the rate levels off at high calcium concentration, suggesting that CaM dissociation by calcium is not a simple second order reaction. Instead we modeled it with the mechanism described within the *dashed-line box* in Fig. 6, except that the conversion of state 2 to state 3 is now considered to be irreversible. Calcium first binds reversibly to a bound CaM. For simplicity, only one calcium ion is shown, but it might take more than one calcium cation to dissociate CaM. MyoV with a bound Ca^{2+} -CaM is still processive (state 2). In the second step, the Ca^{2+} -CaM dissociates from the myosin V neck and generates a nonprocessive myoV (state 3), which is modeled as an irreversible step because it terminates a run. The rebinding of CaM will start a new processive run. This model predicts that the dependence of the observed rate of dissociation (k_{obs}) on Ca^{2+} concentration can be described by Equation 2.

$$k_{\text{obs}} = \frac{k_{\text{term2}}[\text{Ca}^{2+}]}{K_3 + [\text{Ca}^{2+}]} \quad (\text{Eq. 2})$$

When the rates from Table 3 are fitted to this equation, $K_3 = 40 \mu\text{M}$ and $k_{\text{term2}} = 4.8 \text{ s}^{-1}$. Compared with the estimated dissociation constant of $\approx 1\text{--}5 \mu\text{M}$ for the two higher affinity sites of unbound Ca^{2+} -CaM (17, 18), these results suggest that calcium binds at least 10-fold more weakly to bound CaM than to free CaM. By the linked equilibrium in Fig. 6, Ca^{2+} -CaM therefore binds at least 10-fold more weakly than apo-CaM to the heavy chain. An earlier study of CaM affinity to a peptide correspond-

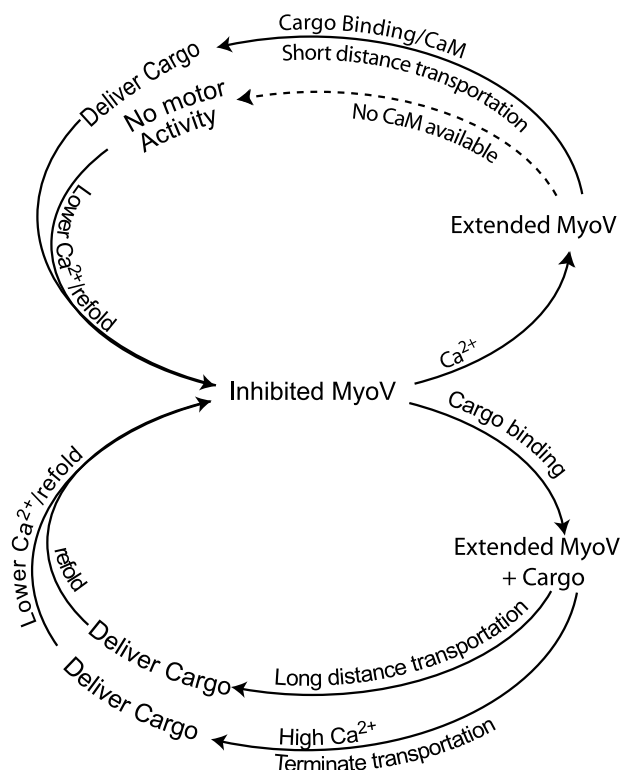


FIGURE 8. Schematic showing multiple pathways for myoV activation and inhibition, which is dependent on both calcium and CaM concentration.

ing to the second IQ motif showed an 8-fold decrease in affinity in the presence of calcium (19). This value might be an underestimate, because additional interactions between adjacent CaMs in the native neck could enhance the binding affinity.

Effect of Actin on the Folded-to-Extended Transition—One head of myoV in the folded form can be docked onto actin, and negatively stained images confirm that the folded monomer can bind to actin (10). If the extended form binds more tightly to actin than the folded form because of two-headed *versus* one-headed binding, then actin binding would favor the extended form. The rate of the extended-to-folded transition may also be slowed by actin binding. Our data show that in EGTA, the characteristic run length of the full-length myoV is approximately half that of dHMM. If we assume that an unfolded full-length myoV has the same characteristic run length as dHMM, and that the reduction of the run length is because of formation of the folded conformation, we can estimate that the rate of folding is $\approx 1 \text{ s}^{-1}$. This value is estimated from the rate of k_{term2} when the observed run length is half of the maximum (Table 3). Assuming an equilibrium constant of 8, the rate of unfolding is therefore $\approx 0.12 \text{ s}^{-1}$. We speculate that in the absence of actin, the rate of the extended to folded transition would be higher.

Myosin V Regulation

Implications for *in Vivo* Regulation of *myoV*—Our results show that the processivity of full-length *myoV* is tightly controlled by the concentration of calcium and CaM. How does this fit into the regulation of *myoV in vivo*? In terms of activation, processive runs could be initiated at low calcium by cargo binding, which disrupts the head-cargo domain interaction, or by a small increase in calcium, which unfolds the molecule (Fig. 8). It is assumed that the calcium concentration needed to activate the full-length molecule is lower than that needed to dissociate a CaM. Once activated, even if a *myoV* molecule with its cargo dissociates from one actin filament, the *myoV* can easily hop onto another actin filament in the cytoskeletal meshwork of actin and continue going until it has reached its intended destination.

The cell then needs a reliable way to turn off the processive run of the motor-cargo complex once it reaches its final destination. Processive runs could be terminated by cargo release at low calcium, which will allow the molecule to refold to the inhibited conformation. Alternatively, a transient increase of calcium could stop the processive run of *myoV* by releasing a CaM and abolishing the communication between the two heads, which serves as a signal for the termination of transportation. The calcium concentration needed for this effect also depends on the local CaM concentration. If little free CaM is present, 1 μM calcium should be sufficient to stop cargo transport. In the presence of 12 μM CaM, a higher calcium concentration ($>10 \mu\text{M}$) is needed to achieve this effect. Is this high level of calcium plausible in the intracellular milieu? Experiments and simulations show the existence of intracellular calcium microdomains with transiently elevated calcium concentrations (from several to greater than 100 μM) in a small region of a variety of cells including neurons (reviewed in Ref. 20). Thus, it is plausible that *myoV* could have its run terminated without a global elevation of cytoplasmic calcium levels. It has been proposed that calcium-induced CaM dissociation from *myoV* occurs in chromaffin cells, allowing syntaxin-1A, a t-SNARE that participates in exocytosis, to bind to a vacant IQ motif. The *myoV*-syntaxin complex then anchors a synaptic vesicle to the plasma membrane, thus mediating vesicle fusion and exocytosis (21). To deliver more cargo, the motor must then be recycled, a process that has been proposed to be mediated by an actin treadmill mechanism (10). Therefore, both calcium-dependent and -independent pathways for starting

and stopping a processive run can be envisioned, with the relative contribution of each pathway dependent on cellular conditions.

Acknowledgments—We thank Alex Hodges, Susan Lowey, and all the members of the Trybus laboratory for constructive comments on the manuscript.

REFERENCES

1. Mehta, A. D., Rock, R. S., Rief, M., Spudich, J. A., Mooseker, M. S., and Cheney, R. E. (1999) *Nature* **400**, 590–593
2. Yildiz, A., Forkey, J. N., McKinney, S. A., Ha, T., Goldman, Y. E., and Selvin, P. R. (2003) *Science* **300**, 2061–2065
3. Trybus, K. M. (2005) *Nat. Cell Biol.* **7**, 854–856
4. Nascimento, A. A., Cheney, R. E., Tauhata, S. B., Larson, R. E., and Mooseker, M. S. (1996) *J. Biol. Chem.* **271**, 17561–17569
5. Krementsova, D. N., Krementsova, E. B., and Trybus, K. M. (2004) *J. Cell Biol.* **164**, 877–886
6. Nguyen, H., and Higuchi, H. (2005) *Nat. Struct. Mol. Biol.* **12**, 127–132
7. Trybus, K. M., Krementsova, E., and Freyzon, Y. (1999) *J. Biol. Chem.* **274**, 27448–27456
8. Wang, F., Thirumurugan, K., Stafford, W. F., Hammer, J. A., III, Knight, P. J., and Sellers, J. R. (2004) *J. Biol. Chem.* **279**, 2333–2336
9. Li, X. D., Mabuchi, K., Ikebe, R., and Ikebe, M. (2004) *Biochem. Biophys. Res. Commun.* **315**, 538–545
10. Liu, J., Taylor, D. W., Krementsova, E. B., Trybus, K. M., and Taylor, K. A. (2006) *Nature* **442**, 208–211
11. Cheney, R. E., O'Shea, M. K., Heuser, J. E., Coelho, M. V., Wolenski, J. S., Spreafico, E. M., Forscher, P., Larson, R. E., and Mooseker, M. S. (1993) *Cell* **75**, 13–23
12. Forkey, J. N., Quinlan, M. E., Shaw, M. A., Corrie, J. E., and Goldman, Y. E. (2003) *Nature* **422**, 399–404
13. Pardee, J. D., and Spudich, J. A. (1982) *Methods Enzymol.* **85**, 164–181
14. Krementsova, E. B., Hodges, A. R., Lu, H., and Trybus, K. M. (2006) *J. Biol. Chem.* **281**, 6079–6086
15. Sakamoto, T., Amitani, I., Yokota, E., and Ando, T. (2000) *Biochem. Biophys. Res. Commun.* **272**, 586–590
16. Baker, J. E., Krementsova, E. B., Kennedy, G. G., Armstrong, A., Trybus, K. M., and Warshaw, D. M. (2004) *Proc. Natl. Acad. Sci. U. S. A.* **101**, 5542–5546
17. Burger, D., Stein, E. A., and Cox, J. A. (1983) *J. Biol. Chem.* **258**, 14733–14739
18. Cox, J. A. (1988) *Biochem. J.* **249**, 621–629
19. Martin, S. R., and Bayley, P. M. (2004) *FEBS Lett.* **567**, 166–170
20. Rizzuto, R., and Pozzan, T. (2006) *Physiol. Rev.* **86**, 369–408
21. Watanabe, M., Nomura, K., Ohyama, A., Ishikawa, R., Komiya, Y., Hosaka, K., Yamauchi, E., Taniguchi, H., Sasakawa, N., Kumakura, K., Ushiki, T., Sato, O., Ikebe, M., and Igarashi, M. (2005) *Mol. Biol. Cell* **16**, 4519–4530